ELSEVIER

Chemical Geology 197 (2003) 143–159

CHEMICAL GEOLOGY
INCLUDING
ISOTOPE GEOSCIENCE

www.elsevier.com/locate/chemgeo

Do fluid inclusions preserve $\delta^{18}O$ values of hydrothermal fluids in epithermal systems over geological time? Evidence from paleo- and modern geothermal systems, Milos island, Aegean Sea

J. Naden[a,b,*], S.P. Kilias[a], M.J. Leng[c], I. Cheliotis[d], T.J. Shepherd[b]

[a] *Section of Economic Geology and Geochemistry, Department of Geology, National and Kapodistrian University of Athens, Panepistimioupolis, Ano Ilisia, 157 84 Athens, Greece*
[b] *British Geological Survey, Keyworth, Notts NG12 5GG, UK*
[c] *NERC Isotope Geosciences Laboratory, British Geological Survey, Keyworth, Notts NG12 5GG, UK*
[d] *Institute for Geology and Mineral Exploration, 70 Messoghion St., 115 27 Athens, Greece*

Received 19 December 2001; accepted 27 September 2002

Abstract

Stable isotope compositions of quartz ($\delta^{18}O_{quartz}$) and fluid inclusion waters ($\delta^{18}O_{FI}$ and δD_{FI}) were analysed from Profitis Ilias, a low-sulphidation epithermal gold mineralisation deposit on Milos island, Greece, to establish if $\delta^{18}O_{FI}$ preserve a record of paleogeothermal processes. Previous studies show that mineralisation at Profitis Ilias resulted from extreme boiling and vaporisation with a zone located at approximately 430 m above sea level (asl) representing the transition between liquid- and vapor-dominated systems [Miner. Depos. 36 (2001) 32]. The deposit is also closely associated with an active geothermal system, whose waters have a well-characterised stable isotope geochemistry [Pflumio, C., Boulegue, J., Liakopoulos, A., Briqueu, L., 1991. Source, Transport and Deposition of Metals. Balkema, Rotterdam]. The samples were collected over an elevation interval of 440 m (210–650 m asl) to give information on the liquid and vapor dominated sections of the paleosystem.

The data show systematic variations with sample elevation. Samples from the highest elevations (ca. 650 m asl) have the lightest $\delta^{18}O_{FI}$ (−7.3‰) and δD_{FI} (−68.0‰) whilst the deepest (ca. 210 m asl) are isotopically heavier ($\delta^{18}O_{FI}$, −0.3‰; δD_{FI}, −19.0‰). Relative changes in $\delta^{18}O_{FI}$ closely parallel those in δD_{FI}. $\delta^{18}O_{quartz}$ shows an opposite trend, from the lightest values (+13.9‰) at the lowest elevations to the heaviest (+15.1‰) at the highest elevations. $\delta^{18}O_{FI}$ shows correlations with other parameters. For example, variable fluid inclusion homogenisation temperatures in the vapor-dominated part of the system correlate with a rapid shift in δD_{FI} (−33.3‰ to −50.5‰) and $\delta^{18}O_{FI}$ (−4.1‰ to −6.2‰). Gold contents also increase in the same zone (up to 50 ppm Au). Comparable correlations in $\delta^{18}O_{quartz}$ or $\delta^{18}O_{calculated}$ (estimated geothermal fluid from fluid inclusion homogenisation data) are absent. $\delta^{18}O_{calculated}$ are always 5–10‰ heavier than $\delta^{18}O_{FI}$. Comparison with the present day geothermal field shows that δD_{FI} and $\delta^{18}O_{FI}$ are similar. Isotope data for the modern system and fluid inclusion waters fall on linear trends subparalleling the meteoric water line and project towards seawater values. Numerical modelling favours kinetically controlled fractionation to explain differences in $\delta^{18}O_{calculated}$ and $\delta^{18}O_{fluid}$ rather than diffusive posttrapping reequilibration. The evidence suggests that in low-temperature epithermal systems, $\delta^{18}O_{FI}$ may represent

* Corresponding author. British Geological Survey, Keyworth, Notts NG12 5GG, UK. Tel.: +44-115-936-3280; fax: +44-115-936-3200.
E-mail address: jna@bgs.ac.uk (J. Naden).

0009-2541/02/$ - see front matter
doi:10.1016/S0009-2541(02)00289-9

a better record of fluid process and the isotopic composition of the paleogeothermal fluid than temperature-corrected quartz data.

Keywords: Fluid inclusions; Oxygen and hydrogen isotopes; Active Aegean arc; Epithermal mineralisation

1. Introduction

Stable isotope analyses (δD and δ^{18}O) of inclusion fluids and minerals provide valuable insights into fluid sources, hydrothermal processes and fluid–rock interaction in a wide range of geological environments (e.g. O'Reilly et al., 1997; Wilkinson et al., 1995). One of the main methodologies for determining D/H and $^{18}O/^{16}O$ focuses on measuring δD on extracted inclusion fluids and calculating δ^{18}O of the fluid by analysing the host quartz. Recently, procedures that analyse both δD and δ^{18}O on inclusion fluids have been developed for quartz and carbonates (Kishima and Sakai, 1980; Kazahaya and Matsuo, 1984; Ohba and Matsuo, 1988; Lecuyer and O'Neil, 1994). However, in quartz, scientific opinions as to which approach is the most appropriate are divided (Vityk et al., 1993; Ohba et al., 1995). The indirect approach is not ideal as it relies on accurate determination of quartz precipitation temperatures, usually ascertained through fluid inclusion microthermometry. Also, there is evidence for isotopic disequilibrium between quartz and the fluid phase at low temperatures (<250 °C) (Zhang et al., 1989; Matsuhisa et al., 1978). Direct measurements also have problems since isotopic reequilibration can occur after trapping and during cooling of the host mineral (Rye and O'Neil, 1968; Ohba et al., 1995).

In this study, we present directly and indirectly measured δD and δ^{18}O data for adularia–sericite epithermal-Au mineralisation at Profitis Ilias on Milos island (Aegean sea); a deposit closely linked to a modern geothermal reservoir, and whose geology, mineralogy and fluid inclusions, are well characterised (Kilias et al., 2001). In addition, the modern system is well documented mineralogically, geochemically and isotopically (Liakopoulos, 1987; Liakopoulos et al., 1991; Pflumio et al., 1991; Christanis and St. Seymour, 1995), and provides an excellent analogue for the epithermal Au mineralisation.

2. Geological setting and background information

2.1. The geology of Milos island

Milos is located on the active Aegean volcanic arc (Fig. 1). Volcanism on Milos is Pliocene to Pleistocene in age and calc-alkaline in nature, and resulted from the northeastward subduction of the Mediterranean seafloor (part of the African plate) below the Aegean microplate (Papazachos and Kiratzi, 1996 and references therein). The geology, geochronology, geothermal activity and structure of the island are described in detail by Fytikas (1989 and references therein), Briqueu et al. (1986), Liakopoulos et al. (1991) and Tsokas (1996), and its main geological features are shown in Fig. 1. Though the last recorded volcanism ceased 100,000 years ago, Milos is currently an active geothermal field. Present-day activity is concentrated in the central and eastern portions of the island and is expressed by fumaroles, hot springs, hot ground and submarine gas escapes (Fig. 1).

2.2. Epithermal gold mineralisation at Profitis Ilias

The geology, mineralogy and fluid inclusions of Profitis Ilias have been described in detail by Kilias et al. (2001), and only the salient features are reiterated here.

The mineralisation is classified as a low-sulphidation epithermal gold deposit and the host rocks consist of strongly sericitised rhyolitic lapilli-tuffs and ignimbrites. The mineralisation, comprising native gold, minor sphalerite, galena, chalcopyrite and pyrite, is developed in a series of interconnected N–S to NE–SW trending vein structure that occupy a fault network. Vein widths are up to 3 m across and extend to depths of at least 300 m below the present-day surface. Three broad paragenetic stages to the mineralisation are recognised: (i) barren pre-ore comprising microcrystalline quartz and pyrite; (ii) fine-grained

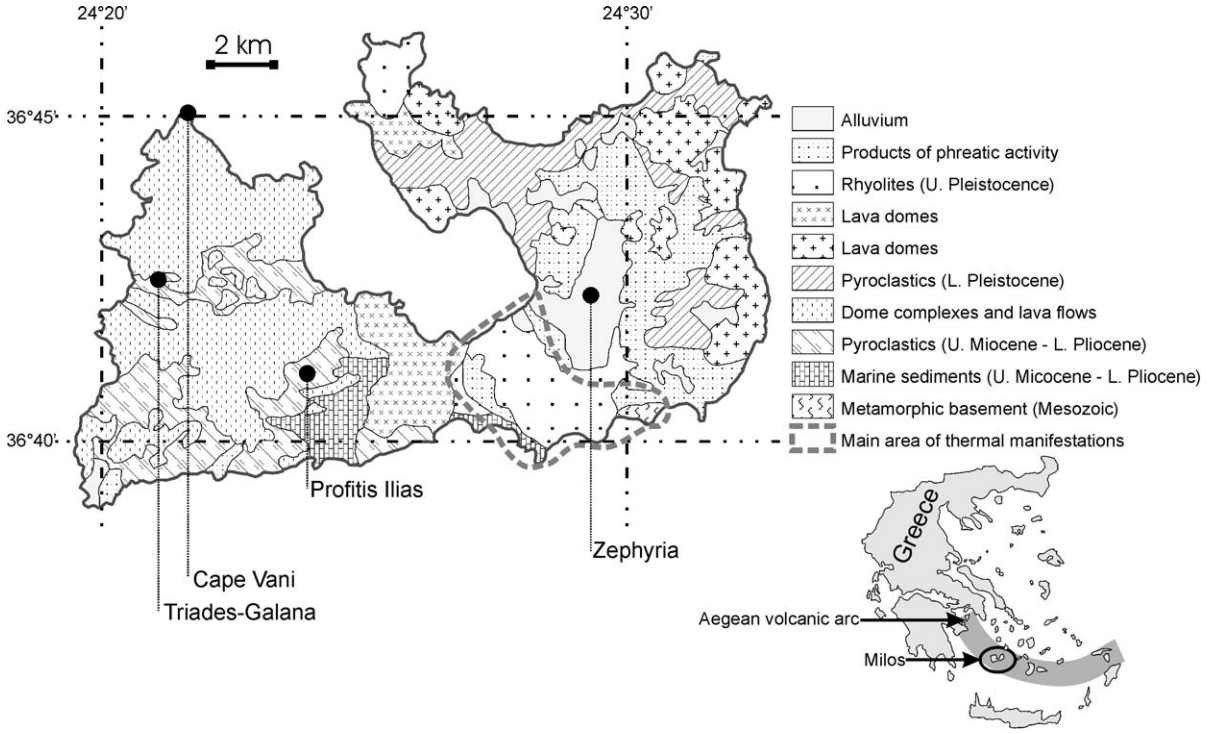

Fig. 1. Geological map of Milos island showing its position on the Aegean arc plus the locations of mineralisation and the geothermal manifestations (modified after Fytikas, 1989).

and vuggy quartz with base metal sulphides and native gold and (iii) post-ore fine-grained quartz and barite with minor to trace sulphides.

Fluid inclusion homogenisation temperatures show either show narrow (25–50 °C) or large ranges (>150 °C) that are not evenly distributed throughout the depth profile. In the lower levels of the hydrothermal system (below 430 m above sea level (asl)), only the narrow range is observed, whilst above this level, samples exhibiting widely varying temperatures predominate (Table 1). In terms of T_h–salinity relationships, the data display two distinct trends:

1. A *high-salinity trend*, where rapidly increasing salinity (3–15 wt.% NaCl eq.) is associated with gradual decreases in homogenisation temperature. This trend is seen throughout hydrothermal system.
2. *High-T_h trend*, where a slight tendency of decreasing salinity is associated with increasing temperature. This trend only occurs in the upper parts of the hydrothermal system (>430 m asl).

In addition to the above, the lowest homogenisation temperatures at each sample depth closely follow a depth-to-boiling curve. This feature is seen in modern geothermal systems (e.g. Hedenquist et al., 1992; Lüders et al., 2001) and provides a reference curve for estimating quartz precipitation temperatures (Table 1).

Kilias et al. (2001) concluded that the fluid inclusion data coupled with geochemical data strongly imply that extreme boiling and vaporisation played a major role in mineralisation. In addition, they noted that a zone, located at approximately 430 m asl, marks the transition between a liquid- and vapor-dominated system. These results show that the studied samples, at the deposit scale, can be treated as being temporally and compositionally consistent and provide a coherent framework to interpret the stable isotope data.

Table 1
Sample information and stable isotope results

Sample no.	Elevation (m asl)	Sample weight (g)	FI water weight (mg)	$\delta^{18}O_{quartz}$ (‰)	$\delta^{18}O_{FI}$ (‰)	δD_{FI} (‰)	Salinity (wt.% NaCl eq.)	T_h range (°C)	Boiling curve T (°C)
G2185	657	1.4	0.5	15.4	−4.5	−28.7	6.1–6.8	150–160	89
G1746	621	0.5	2.5	15.5	−7.8	−51.0	5.0–5.5	213–243	149
G1810	613	0.5	0.3	15.1	−7.3	−47.8	4.5–4.5	161–284	156
G2374	551	1.5	1.2	14.2	−7.8	−68.0	3.4–5.6	190–234	188
G2245	499	0.5	3.7	14.6	−6.9	−41.5	3.3–4.9	205–215	204
G2255	457	0.5	1.6	13.9	−6.1	−39.8	3.1–4.7	190–219	213
G2424	421	0.7	1.2	14.2	−6.2	−50.5	0.0–7.5	233–253	220
G2267	405	1.4	3.7	14.3	−4.1	−33.3	6.5–7.8	223–249	223
G2268	403	1.2	2.5	13.7	−4.5	−34.9	4.4–9.2	208–231	223
G2283	365	1.2	0.3	13.4	−3.7	−23.8	3.1–6.2	219–251	230
PD9380	210	0.5	1.2	14.5	−0.3	−19.0	5.6–5.6	237–280	250

Also shown are summary microthermometric data and boiling curve temperatures for each sample elevation (from Kilias et al., 2001).

2.3. The modern geothermal system: chemical and isotopic characteristics

In the active geothermal system, the reservoir liquid before phase separation is moderately saline (~ 9 wt.% dissolved salts), and after phase separation, the condensed vapor has a salinity of 0.12 wt.% NaCl. Geochemically, the residual liquid phase is dominated by sodium chloride (up to 14.3 wt.% NaCl) with significant potassium (1.1 wt.%) and calcium (0.5 wt.%). In addition, magnesium (1.36×10^{-4} mol l^{-1}) and sulphate (1.04×10^{-5} mol l^{-1}) are strongly depleted compared to seawater. During its ascent to the surface, the hydrothermal fluid separates into liquid and vapor phases (Liakopoulos, 1987; Liakopoulos et al., 1991). In terms of stable ($\delta^{18}O$, δD) isotope systematics, the deep reservoir comprises a fluid that resulted from a Rayleigh-type distillation of seawater accompanied by partial reequilibration with volcanic rocks as the seawater percolated down through the system (Pflumio et al., 1991).

3. Materials and methods

3.1. Sample selection and preparation

Sample selection for isotopic analysis was based on fluid inclusion microthermometry and elevation data. The criteria were that quartz samples contained only a single-inclusion type with an inclusion population dominated by primary/pseudosecondary inclusions and that they covered most of the vertical range of the deposit. In total, 11 quartz samples were selected for analysis (Table 1). Approximately 10 g of quartz from each sample were crushed and sieved to $-1000+500$ μm. The quartz concentrates were then washed in hot (ca. 90 °C) 6 M HCl several times with a final rinse in hot (ca. 90 °C) Milli Q water to remove "soluble" impurities adhering to the surface of the quartz grains (e.g. iron oxides). This was followed by ultrasonic cleaning in cold Milli Q water for 5 min to remove "insoluble" surface impurities (e.g. clay minerals). Any contaminants left were then removed by careful handpicking under a binocular microscope to give a pure quartz concentrate weighing between 0.5 and 1.0 g. Immediately, prior to analysis, the sample was briefly ultrasonically cleaned in dichloromethane to remove any remaining organic material.

3.2. $\delta^{18}O$ and δD from fluid inclusions

$\delta^{18}O$ and δD in fluid inclusions were determined using a modified methodology based on Kishima and Sakai (1980), Kazahaya and Matsuo (1984) and Lecuyer and O'Neil (1994). Between 0.5 and 1 g of handpicked quartz grains were degassed at ~ 20 °C overnight under vacuum. Samples were then decrepitated at 600 °C for 30 min and the fluid inclusion water collected cryogenically. This water was then transferred to a microequilibration quartz tube sealed

at one end, to which 2 cm^3 of a standard CO_2 gas was added, and the tube completely sealed. The tube was then weighed, and the H_2O and standard CO_2 gases were left to exchange oxygen isotopes at 25 °C for 7 days. After equilibration, H_2O and CO_2 were separated cryogenically. The water was converted to hydrogen by reduction over hot zinc and ratios were measured on a SIRA 10 mass spectrometer. CO_2 was collected and ratios were determined on an Optima mass spectrometer along with a sample of the standard gas used for the equilibration. The $\delta^{18}O$ values of the water samples were calculated using the mass balance equation of Kishima and Sakai (1980) and the CO_2–H_2O fractionation factor at 25 °C was determined using O'Neil et al. (1975). The $\delta^{18}O$ value of standard CO_2 used for equilibration was 31.85‰ (SMOW), a value close to that expected for the CO_2 after equilibration. Since the oxygen isotope ratio of the CO_2 only changes slightly during the equilibration, the precision was not compromised. The weight of fluid inclusion water released from the quartz was calculated from the weights of the collection tubes before and after the H_2O–CO_2 collection. The water content of each sample was variable, but in most cases, 0.5–1 g of quartz yielded between 0.5 and 4 μl of water (Table 1). At each stage in the extraction procedure, the line pressure was monitored to check for residual gas. Precisions obtained for the laboratory-standard water, extracted and measured at the same time, were 0.1‰ for $\delta^{18}O$ and 3‰ for δD (2σ) for samples containing between 1 and 2 μl of water. The data are presented as per mil (‰) deviations from VSMOW.

3.3. $\delta^{18}O$ from quartz

Silicate ratios were obtained from the quartz after fluid inclusion extraction using the procedure outlined by Clayton and Mayeda (1963). Oxygen yields were monitored and considered acceptable within the range 99–103% of the theoretical yield. Isotope ratios were measured on a CJS Sciences mass spectrometer (phoenix 390, rebuilt VG MM903). $\delta^{18}O$ values were normalised through laboratory standards and NBS28, and corrected according to Craig (1957) and Deines (1970). The data are presented as per mil (‰) deviations from VSMOW. Overall, analytical reproducibility was of the order of ±0.10‰ (2σ).

4. Stable isotope results

4.1. Oxygen data

The oxygen isotope data show correlations between sample elevation and $\delta^{18}O$ in both fluid inclusion waters ($\delta^{18}O_{FI}$) and quartz ($\delta^{18}O_{quartz}$) (Table 1 and Fig. 2). With the exception of the sample from the highest elevation, $\delta^{18}O_{FI}$ decreases from −0.3‰ at 210 m asl to −7.3‰ at 613 m asl. $\delta^{18}O_{quartz}$ shows an opposite trend, increasing from +13.4‰ to +15.1‰. However, to directly compare the quartz and fluid inclusion water data, $\delta^{18}O_{quartz}$ needs to be corrected for temperature-dependent fractionation effects between quartz and the hydrothermal fluid ($\delta^{18}O_{corrected}$). However, in low- to moderate-temperature epithermal systems (<250 °C), correct estimation of quartz precipitation temperatures from fluid inclusion temperatures can be difficult and errors in temperature estimate can result in significant uncer-

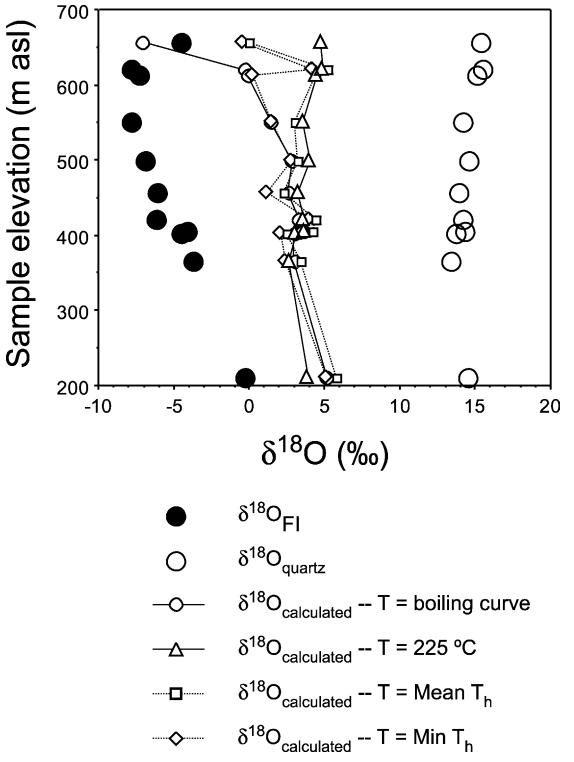

Fig. 2. Plot of sample depth versus $\delta^{18}O$ comparing values obtained from inclusion water, quartz and $\delta^{18}O$ calculated from fluid inclusion temperatures (see text for discussion).

tainties in isotopic compositions. At 200 °C, an uncertainty of ±20 °C for example in the fluid inclusion homogenisation temperature corresponds to a 2.5‰ uncertainty in $\delta^{18}O_{fluid}$. Furthermore, at Profitis Ilias, where there is a temperature difference of approximately 100 °C between the lowest and highest elevations, uncertainties of this magnitude are greater than the total range in the measured quartz oxygen isotopic composition (1.2‰). Several choices of temperature estimate are available to us. First, there is a single value, e.g. 225 °C, that corresponds to estimated boiling temperatures, but there is a clear variation in temperature over the investigated elevation interval (see Table 1). Second, average sample homogenisation temperatures (Table 2) could also be appropriate. However, in this case, there is good evidence for heterogeneous trapping (Kilias et al., 2001), which will make this choice an overestimation. Third, the minimum homogenisation temperature of each sample (Table 1), which represents fluid inclusions that have trapped the least vapor, is also a valid estimate (see Pichavant et al., 1982; Ramboz et al., 1982; Bodnar et al., 1985 for discussions that relate homogenisation temperatures, boiling and heterogeneous trapping). Last, we have depth-to-boiling relationships to estimate fluid temperatures (Table 1).

Fig. 2 compares $\delta^{18}O_{corrected}$, $\delta^{18}O_{FI}$ and $\delta^{18}O_{quartz}$ with sample elevation using the above methods for estimating temperature. First, it is clear that trends in the data are systematically related to sample elevation. Second, there is a difference of about +8‰ to +12‰ between $\delta^{18}O_{FI}$ and $\delta^{18}O_{corrected}$. Closer examination of the corrected data raises a number of further points:

1. Use of a single temperature value preserves the $\delta^{18}O$–depth trend seen in the quartz data, which is still in the opposite sense to the inclusion water data.
2. Employing mean homogenisation temperature results in significant scatter, and makes it difficult to differentiate any data trends.
3. Minimum homogenisation temperature again results in scatter, but trends in the data are now discernible and the $\delta^{18}O$–depth trend is in a similar sense to that of the inclusion water.
4. Applying temperature estimates calculated from the boiling curve, with the exception of the sample from the highest elevation, results in a trend with little scatter that closely parallels the inclusion water.

4.2. Hydrogen data

δD of inclusion waters (δD_{FI}) varies between −68.0‰ and −19.0‰. δD_{FI} shows a reasonable correlation with sample elevation (Fig. 3), with eight of the eleven samples analysed falling on a linear trend varying from the light values (−47.8‰) at high elevations (613 m asl) to heavier values (−19‰) at lower altitudes (210 m asl).

Table 2
Comparison of fluid inclusion water $\delta^{18}O$ with calculated fluid compositions for Profitis Ilias

Sample no.	Elevation (m asl)	$\delta^{18}O_{FI}$ (‰)	$\delta^{18}O_{quartz}$ (‰)	$\delta^{18}O_{calculated}$ (‰) (T=boiling curve)	$\delta^{18}O_{calculated}$ (‰) (T=225 °C)	$\delta^{18}O_{calculated}$ (‰) (T=mean T_h)	Boiling curve T (°C)	Mean T_h (°C)
G2185	657	−4.5	15.4	−7.1	4.8	0.0	89	155
G1746	621	−7.8	15.5	−0.3	4.9	5.2	149	230
G1810	613	−7.3	15.1	−0.1	4.5	4.4	156	223
G2374	551	−7.8	14.2	1.4	3.6	3.0	188	214
G2245	499	−6.9	14.6	2.8	4.0	3.2	204	211
G2255	457	−6.1	13.9	2.6	3.3	2.3	213	207
G2424	421	−6.2	14.2	3.3	3.6	4.4	220	241
G2267	405	−4.1	14.3	3.6	3.7	4.2	223	234
G2268	403	−4.5	13.7	3.0	3.1	2.5	223	215
G2283	365	−3.7	13.4	3.0	2.7	3.4	230	238
PD9380	210	−0.3	14.5	5.1	3.9	5.8	250	264

Calculated fluids use Zhang et al. (1989).

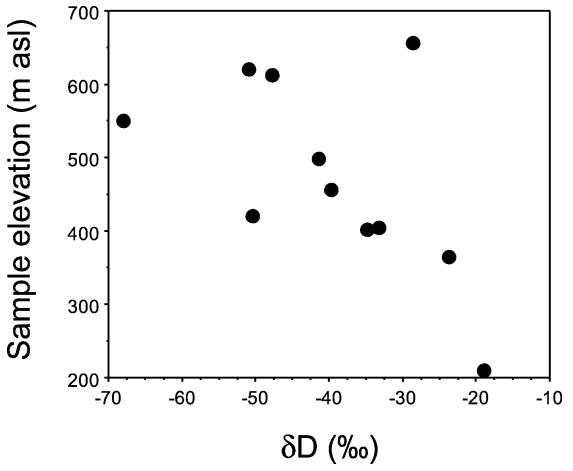

Fig. 3. Graph of δD versus sample elevation, showing a general trend of increasing δD with increasing sample depth.

4.3. Correlations between stable isotope, fluid inclusion and geochemical data

In addition to isotope elevation data, it is also possible to examine the relationships between stable isotope, fluid inclusion and geochemical data (Au and Ag). It is clear that 430 m asl marks a distinct transition (Fig. 5). First, δD and $\delta^{18}O_{FI\ water}$ show a significant decrease to lighter values and relative changes in δD closely parallel those in $\delta^{18}O_{FI\ water}$. Second, fluid inclusion homogenisation temperatures start to show a high degree of variability above 430 m asl. Here, individual samples commonly record T_h ranges in excess of 100 °C, whilst below the transition temperature, ranges are generally less than 20 °C. This variation correlates with the shift in $\delta^{18}O_{FI}$ and δD_{FI} to lighter values. Third, at 430 m asl, metal contents start to increase and gold contents are commonly greater than 20 ppm. In comparison, the variation in $\delta^{18}O_{quartz}$ shows a gradual change along the entire depth profile and there is no clearly marked change at 430 m asl.

5. Discussion

5.1. Combined δD and δ^{18}O, and comparisons with the modern geothermal system

Comparison of the paleo- and modern systems on Milos show that $\delta^{18}O_{FI}$ has a number of features in common with present day systematics. It has a similar range in oxygen isotope composition, and combined δD_{FI}–$\delta^{18}O_{FI}$ are close to the vaporisation–mixing trend described by Pflumio et al. (1991) (Fig. 5). In addition, the variation in the isotopic composition of the fluid inclusion waters is modelled by boiling processes. Fig. 5 shows two steam separation trends that match the $\delta^{18}O_{FI}$ data. Here, the heavier samples, in both δD and δ^{18}O, are located at the lowest elevations and are within the liquid-dominated portion of the hydrothermal system (below ~ 430 m asl), and correspond to the highest temperatures in the system. Conversely, the lightest samples are located in the vapor-rich part (above ~ 430 m asl) and have highly variable fluid inclusion temperatures indicative of heterogeneous trapping of liquid and vapor (Figs. 4 and 5). The observed depth–temperature–isotopic variation in $\delta^{18}O_{FI}$ can be explained by the trapping of varying physical mixtures (as fluid inclusions) of residual liquid and steam, with each "quartz extraction" recording an "averaged" isotopic composition. In this manner, samples from the higher elevations will contain more steam and record the lightest δD and δ^{18}O values, whilst those in the deeper portions will be more representative of the reservoir and residual fluid compositions. However, in terms of $\delta^{18}O_{quartz}$ compositions, irrespective of the temperature used to calculate quartz–water fractionation, the $\delta^{18}O_{calculated}$ data plot well to the right of the meteoric water line, in a scattered manner that cannot be related to the modern geothermal system and have no obvious trends.

5.2. The quartz–inclusion water δ^{18}O shift

Table 2 compares $\delta^{18}O_{FI}$ and $\delta^{18}O_{corrected}$ and clearly shows calculated fluid compositions do not equate with those measured in the fluid inclusions. In most cases, irrespective of the choice of temperature, calculated compositions are generally 5–10 ‰ heavier than the measured fluid inclusion waters. To address the reasons for this, let us examine the limited number of cases reported in the literature where both quartz and inclusion water have been analysed (Table 3).

First, Rye and O'Neil (1968) analysed δ^{18}O in inclusion waters hosted in calcite, sphalerite and quartz, and concluded that $\delta^{18}O_{FI}$ undergoes posttrapping exchange with quartz. However, these conclu-

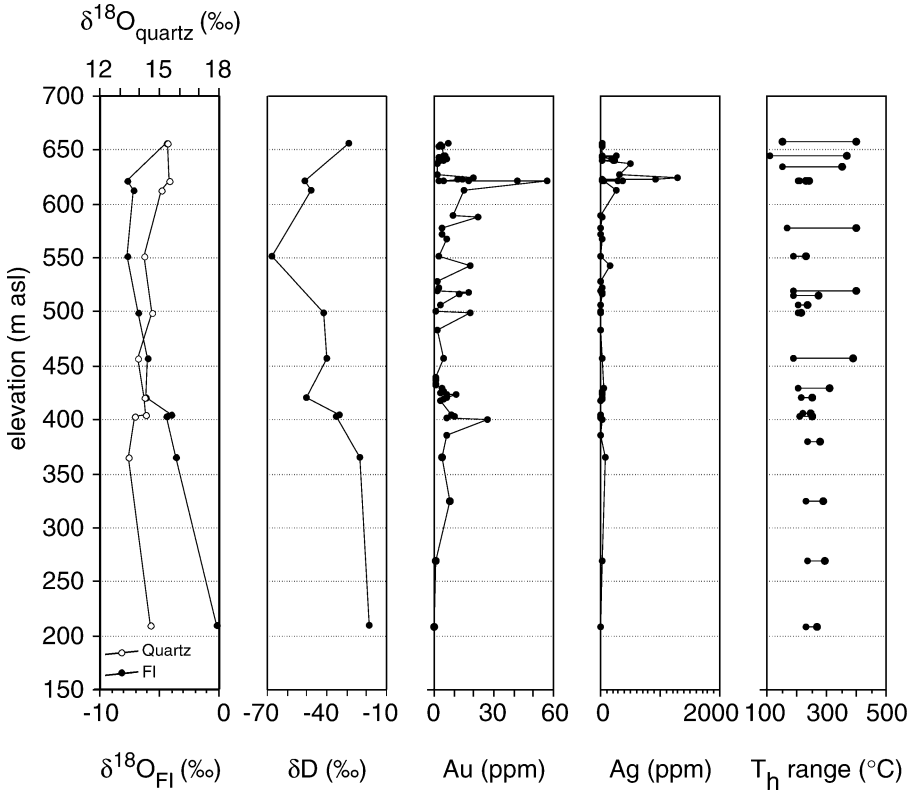

Fig. 4. Combined stable isotope, fluid inclusion and assay graphs, showing how $\delta^{18}O$, δD, fluid inclusion T_h and metal (Au, Ag) content vary with depth, and how they are related to each other. Each parameter shows a distinct change at approximately 430 m asl. Both $\delta^{18}O$ and δD decrease rapidly, fluid inclusion homogenisation temperatures change from showing only a narrow range to being highly variable and gold contents in quartz start to increase and are locally over 30 ppm.

sions are based on limited data and large samples (Table 3). Thus, it is possible that they did not sample a single generation of quartz or fluid. This is important as Hayashi et al. (2001) have shown that in epithermal quartz, $\delta^{18}O_{quartz}$ can vary by up to 7‰ in on a millimetric scale. Thus, without knowing the homogeneity of the material and considering the small number of quartz samples analysed, it is difficult to assess the effects of posttrapping reequilibration from this data alone.

Second, Vityk et al. (1993) and Ohba et al. (1995) analysed both $\delta^{18}O_{FI}$ and $\delta^{18}O_{quartz}$ from the Beregovo epithermal and Kaneuchi tungsten deposits and had significantly different results. Vityk et al. (1993) record two distinct types of quartz and fluid inclusion. In the first, isotope and fluid inclusion temperatures agree and microthermometry indicates a compositionally and thermally homogeneous hydrothermal fluid (salinity: 1–2 wt.% NaCl eq.; T_h: 190–215 °C). In the second, isotope and fluid inclusion temperatures disagree and microthermometric data vary considerably (wt.% NaCl eq.: 0–16 wt.%; T_h: 170–260 °C). Also, fluid inclusion waters extracted from sulphides (sphalerite and galena) and coexisting quartz have very similar $\delta^{18}O_{FI}$ and $\delta^{18}D_{FI}$ (Table 3). These data lead to their conclusion that in epithermal systems, inclusion fluids can preserve $\delta^{18}O$ over geologic time. It is also important to note that Beregovo is a relatively young deposit (ca. 15 Ma).

In contrast, Ohba et al. (1995), for relatively high temperature (300–400 °C) and old (ca. 91 Ma) hydrothermal quartz, show that positive $\Delta^{18}O_{corrected\text{-}FI}$ is due to posttrapping diffusional exchange. However, it is important to note that in both Rye and O'Neil (1968) and Ohba et al. (1995), formation temperatures for hydrothermal quartz were in excess of 300

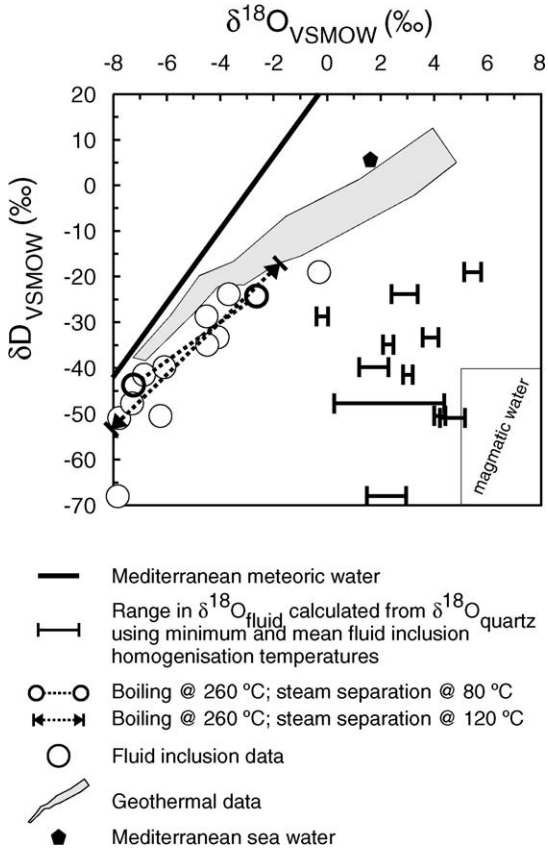

Fig. 5. Combined D/H–δ^{18}O graph comparing directly measured and calculated data with the stable isotope systematics of the modern geothermal system. Included for reference purposes are: (i) two single-stage steam separation trends for fluid with 5 wt.% dissolved NaCl (calculated using the methodology of Truesdell, 1984; the steam tables of Haas, 1977a,b; and the fractionation data of Horita et al., 1995), (ii) the top left part of the magmatic water box (Sheppard, 1986), (iii) the Mediterranean meteoric water line and Mediterranean seawater (see text for discussion of the data).

°C. It is known from experimental work (Matsuhisa et al., 1978; Zhang et al., 1989) that at temperatures in excess of 300 °C, equilibration between quartz and water is relatively rapid (ca. 30–100 h) whilst at temperatures lower than 250 °C, isotopic equilibrium is not achieved. Thus, for both of these studies, due to the high precipitation temperature of the hydrothermal quartz and the time elapsed since mineralisation, some posttrapping exchange by diffusion can be expected. But in lower temperature (<250 °C) young (<15 Ma) epithermal deposits, such as Profitis Ilias and Beregovo, reequilibration by diffusion may not occur. Here, as the quartz cools rapidly from hydrothermal to ambient temperatures, slow δ^{18}O diffusion rates may prevent significant posttrapping exchange. This is indicated qualitatively at Beregovo, where one type of quartz has clearly not undergone any significant posttrapping exchange (Table 3).

5.3. Modelling of posttrapping exchange by diffusion

We can examine posttrapping exchange by diffusion by looking at Dodson closure temperatures (Dodson, 1973, 1979) for δ^{18}O in quartz. This approach is particularly successful in systems dominated by volume diffusion (Valley, 2001) and δ^{18}O diffusion between the wall of a fluid inclusion, and bulk quartz is one example of this.

$$T_c = \left\{ \frac{E/R}{\ln\left(\frac{-ART_c^2(D_0/a^2)}{E(\delta T/\delta t)}\right)} \right\} \quad (1)$$

The Dodson equation (Eq. (1)) defines the closure temperature (T_c [K]) in terms of a dimensionless diffusional anisotropy parameter (A), the gas constant (R [J mol^{-1} K^{-1}]), the preexponential diffusion coefficient (D_0 [m^2 s^{-1}]), activation energy (E [J]), distance over which diffusion takes place (a [m]) and cooling rate ($\delta T/\delta t$ [K s^{-1}]). As individual fluid inclusions generally have small volumes (<0.125 μl), then diffusion and exchange of δ^{18}O between host quartz and inclusion water over short distances will significantly effect the composition of inclusion water. For example, a 1-μm-thick shell of quartz surrounding 10 μm of spherical fluid inclusion represents over 70% of the inclusion volume (Fig. 6A). Thus, it is necessary to examine closure temperatures for diffusion distances at the micron and submicron scale. Fig. 6B shows quartz closure temperatures at a variety of diffusion distances and cooling rates. From this, it is clear that the closure temperature of δ^{18}O in quartz, even for very short distances (ca. 0.01 μm), is higher than most epithermal mineralisation (ca. 250 °C) for cooling rates in excess of ca. 100 °C Ma^{-1}. This means that in low- to moderate temperature

Table 3
Data from previous inclusion water–quartz $\delta^{18}O$ studies

Data source	Sample no.	Sample wt. (g)	FI water wt. (mg)	$\delta^{18}O_{FI}$ (‰)	$\delta^{18}O_{quartz}$ (‰)	$\delta^{18}O_{calculated}$ (‰)	$\Delta^{18}O_{calculated\ FI}$ (‰)	Temperature (°C)	δD_{FI} (‰)
Rye and O'Neil (1968)	63-R-4	60.6	6.0	−3.7	n.a.	–	–	–	n.a.
	63-R-23	29.5	6.2	−4.5	15.8	8.4	12.9	300	n.a.
	63-R-23	29.5	6.2	−4.5	15.8	9.0	13.5	315	n.a.
Ohba et al. (1995)	G-1	n.g.	n.g.	−0.3	n.a.	–	–	–	n.a.
	G-2	n.g.	n.g.	−1.1	14.5	7.1	8.2	300	n.a.
	G-2	n.g.	n.g.	−1.1	14.5	9.9	11.0	400	n.a.
	G-3	n.g.	n.g.	−5.8	14.5	7.1	12.9	300	n.a.
	G-3	n.g.	n.g.	−5.8	14.5	9.9	15.7	400	n.a.
	Y-1	n.g.	n.g.	−11.2	14.2	6.8	18.0	300	n.a.
	Y-1	n.g.	n.g.	−11.2	14.2	9.6	20.8	400	n.a.
Vityk et al. (1993)	486 QI	3–5	n.g.	−5.6	9.2	−2.9	2.7	200	−72
	1308 QI	3–5	n.g.	−5.0	7.5	−2.8	2.2	230	−80
	1522 QI	3–5	n.g.	−5.9	9.7	0.3	6.2	250	−79
	496 QII	3–5	n.g.	−7.1	8.7	−2.8	4.3	210	−56
	523 QII	3–5	n.g.	−1.9	9.4	−2.7	−0.8	200	−66
	515 QII	3–5	n.g.	−2.4	8.7	−2.8	−0.4	210	−79
	483 QII	3–5	n.g.	−2.8	9.1	−3.0	−0.2	200	−84
	A	n.g.	n.g.	−3.5	–	–	–	–	−82
	B	n.g.	n.g.	−2.5	–	–	–	–	−79
	477 QII	3–5	n.g.	−4.0	8.7	−3.4	0.6	200	−94
	100 QIII	3–5	n.g.	−2.1	15.1	4.8	6.9	230	−55
	331 QIII	3–5	n.g.	−0.9	17.9	7.6	8.5	230	−52

Calculated fluid compositions use Zhang et al. (1989).
n.a. = not analysed; n.g. = not given; A = coexisting sphalerite; B = coexisting galena.

epithermal deposits, the $\delta^{18}O$ of inclusion water will not be significantly modified by posttrapping exchange with quartz. However, in higher temperature (300–400 °C) hydrothermal systems, Fig. 6B shows that quartz is not closed to $\delta^{18}O$ diffusion. Hence, posttrapping diffusion will take place and the $\delta^{18}O$ composition of the inclusion water will be modified. Also, in higher temperature systems, the degree of exchange will be dependent on inclusion size. As for a given distance and cooling rate, smaller inclusions will have proportionally more quartz to exchange with than larger inclusions (see Fig. 6A). This relationship between inclusion size and degree of posttrapping exchange has been recorded by Ohba et al. (1995). Thus, for high temperature (>300 °C) hydrothermal systems, $\delta^{18}O_{quartz}$ data coupled with accurate knowledge of quartz precipitation temperatures are better estimators of $\delta^{18}O_{fluid}$ than $\delta^{18}O_{FI}$. However, in lower temperature systems (<250 °C), quartz closure temperatures indicate that fluid inclusions do not reequilibrate with quartz during cooling, and to this, Vityk et al. (1993) show that quartz–fluid inclusion isotope temperatures associated with a specific quartz type are in good agreement with fluid inclusion microthermometry. However, for the Profitis Ilias samples and other quartz types at Beregovo, isotope temperatures do not agree (see Tables 2 and 3). Thus, in the epithermal examples, the fact that some isotope temperatures agree and others do not suggests that another process must be responsible for the differences.

5.4. Kinetically controlled fluid–mineral exchange during quartz formation

Dubinina and Lakshtanov (1997) provide a different perspective into reasons for the quartz–inclusion water $\delta^{18}O$ shift. They show that providing no other isotopic equilibration mechanism operates (e.g. diffusion), complete isotopic equilibrium between a mineral and a fluid phase cannot be achieved through kinetically controlled solution–precipitation pro-

cesses. Dubinina and Lakshtanov (1997) expressed the degree of isotopic exchange (F) between quartz and fluid, where the quartz has a silica gel precursor, as

$$F = \frac{\Delta^0 - \Delta^i}{\Delta^0 - \Delta^e} \quad (2)$$

where Δ^0, Δ^i and Δ^e are differences in δ values between fluid and (i) silica gel (Δ^0), (ii) freshly precipitating quartz (Δ^i) and (iii) quartz at equilibrium (Δ^e). Additionally, they described the degree of exchange (F) in terms of total mass of water (w), total mass of mineral (M) and mass of dissolved and reprecipitated mineral (m) as

$$F = \left[1 - \exp\left(-\frac{m}{w}\right)\right]\left(1 + \frac{w}{M}\right) \quad (3)$$

Eq. (3) means that during solution–precipitation, isotopic fractionation between mineral and fluid can exceed the predicted equilibrium value of $\Delta_{\text{mineral–fluid}}$. This has been recorded experimentally by Zhang et al. (1989) who documented $\Delta^i - \Delta^e$ values of +8.3 ‰ during the early stages of a 250 °C silica gel–water isotope equilibration experiment.

The modelling predicts changes in isotopic composition as an unstable mineral is transformed isochemically into a stable one and is particularly relevant to epithermal systems where crystalline quartz can have amorphous precursors (e.g. Dong et al., 1995). The following equation describes variations in the bulk isotopic composition of quartz ($\bar{\delta}^s_B$) formed during solution–precipitation processes (for a

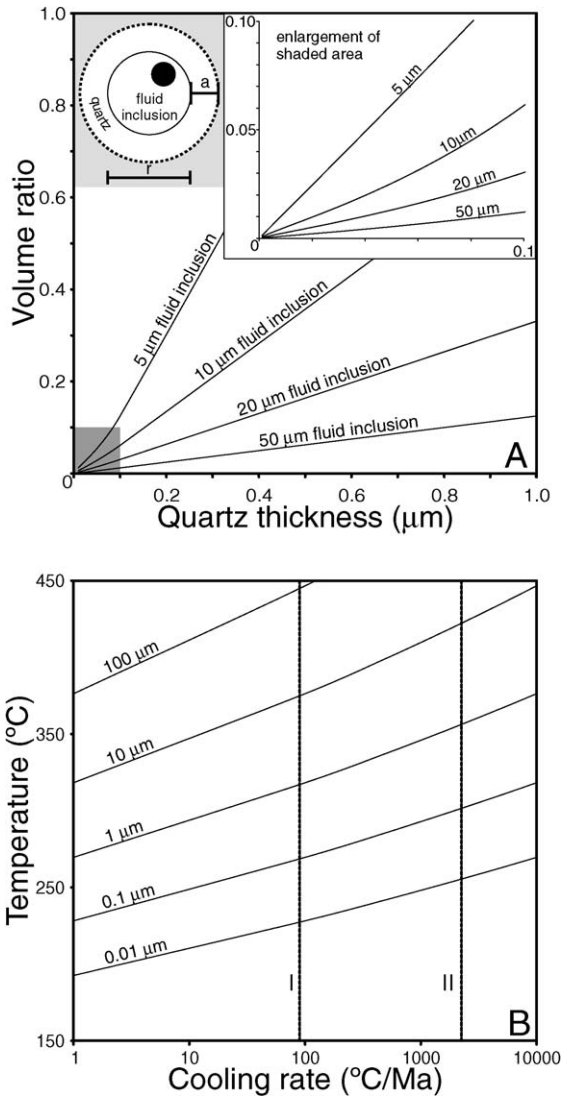

Fig. 6. Inset diagram shows a cross-section through a hypothetical spherical fluid inclusion (diameter r) with a halo of quartz (thickness a) that inclusion water can exchange $\delta^{18}O$ through diffusion. At distances $>a$, the inclusion does not exchange with the quartz. (A) Graph of the volume ratio of a spherical quartz shell and fluid inclusion at different inclusion sizes and quartz shell thicknesses—inset graph shows volume ratio variation at low (<0.1) thicknesses. At low volume ratios (<0.05), any posttrapping diffusive exchange will not significantly affect the isotopic composition of the fluid inclusion as the volume of the inclusion is significantly larger than the amount of quartz available for diffusive exchange. Thus, for inclusions not to be affected by posttrapping exchange, effective diffusion distance must not be greater than ~ 0.01 μm. (B) Graph of Dodson closure temperatures of quartz as a function of effective diffusion distance (a in inset). Line I is a cooling rate reflecting the maximum age and temperature (225 °C) of the Profitis Ilias mineralisation and present-day ambient temperature (25 °C)—this represents the lowest possible cooling rate. Line II reflects a typical life span of a hydrothermal system (100 ka) and a temperature drop of 200 °C (calculations use data of Farver and Yund, 1991 and an infinite cylinder diffusion model). From A and B, it is clear that for diffusion distances in the region of 0.01 μm, the closure temperature for cooling rates applicable to Profitis Ilias (between Line I and II) is greater than the temperature of mineralisation (225 °C).

detailed discussion of its derivation see Dubinina and Lakshtanov, 1997):

$$\bar{\delta}^{s}_{B} = \delta^{0}_{A} - \frac{w}{m}(\Delta^{0} - \Delta^{i})\left[1 - \exp\left(-\frac{m}{w}\right)\right] \quad (4)$$

where δ^{0}_{A} is the initial isotopic composition of the amorphous (unstable) phase, Δ^{0} is derived from the initial isotopic compositions of the fluid (δ^{0}_{w}) and the unstable silica phase ($\Delta^{0} = \delta^{0}_{A} - \delta^{0}_{w}$), Δ^{i} is calculated from the initial fluid composition and quartz–water fractionation at the temperature at which the solution–precipitation process take place ($\Delta^{i} = \delta^{0}_{w} + 1000\mathrm{Ln}_{\alpha}$) and m/w represents the reprecipitated mineral–fluid ratio as the amount of quartz formed (m) changes from 0 to M. To model how kinetic processes relate to our measured quartz compositions, we need to estimate the initial isotopic compositions of the fluid, the unstable silica phase and temperature. A first approximation of solution–precipitation temperatures can be estimated from fluid inclusion data (ca. 225 °C). For the initial fluid, the composition of the modern reservoir (+3‰ , Pflumio et al., 1991) provides a good analogue for the paleosystem at Profitis Ilias. Kita and Taguchi (1986) measured isotopic fractionation factors between colloidal silica and a geothermal fluid at 76 and 88 °C, where silica was allowed to precipitate by evaporation of the geothermal fluid. This is broadly analogous to Profitis Ilias, where mineralisation is associated with extreme boiling and vaporisation, (Kilias et al., 2001). Fig. 7 reproduces their data and compares it with fractionation factors for various equilibrium silica–water pairs. From these studies, it is clear that silica–water oxygen isotope fractionation, under evaporative conditions, is non-equilibrium. Moreover, $\Delta^{18}O_{silica-water}$ appears to increase with temperature. Though it would be difficult to extrapolate these data to higher temperatures, it would be reasonable to use the higher temperature value (+14‰) as a minimum estimate for Δ^{0}. Using the above information and Eq. (4), we can model the bulk isotopic composition of quartz formed from a "colloidal" precursor at 225 °C. Fig. 8A illustrates this approach and three features are evident: (i) the final composition of transformed quartz is dependent on fluid–mineral ratios, (ii) compositions are approximately 3‰ heavier at low mineral–fluid ratios ($w/M = 0.05$) than at isotopic equilibrium and (iii) with $w/M > 10$, kinetic processes start to approximate equilibrium quartz–water fractionation. In terms of our $\delta^{18}O_{quartz}$ data, if we take the deepest and hottest sample (PD9380 in Table 1) to be most representative of the reservoir composition, $\delta^{18}O_{quartz}$ and $\delta^{18}O_{FI}$ can be modelled by solution–precipitation processes. Using Eq. (4), the measured $\delta^{18}O_{quartz}$ (+14.5‰) predicts an initial fluid composition of 0.7‰ ($T = 225$ °C, $w/M = 0.05$, $\delta^{0}_{A} = +14$‰), which is very close to the measured $\delta^{18}O_{FI}$ (−0.3‰), whereas equilibrium fractionation predicts a fluid composition of +3.9‰.

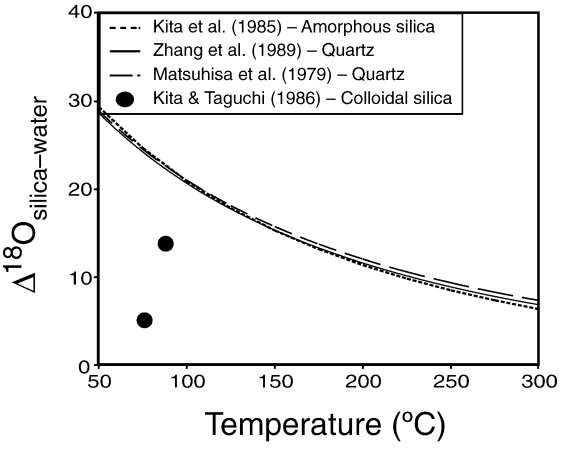

Fig. 7. Silica–water fractionation factors for quartz, amorphous silica and colloidal silica.

At Profitis Ilias, the fluids were boiling and temperatures of quartz formation vary systematically with depth (Table 1). Fig. 8B models this variation and depicts a number of scenarios where $\delta^{18}O_{quartz}$ varies with temperature, w/M, and initial fluid composition (δ^{0}_{w}), and from this, a number of controls on $\delta^{18}O_{quartz}$ can be seen:

1. Where quartz precipitates in equilibrium with a hydrothermal fluid ($\delta^{0}_{w} = 1$‰), which varies in temperature from 250 to 100 °C. $\delta^{18}O_{quartz}$ shows a relatively large systematic variation from 9.9‰ to 22.0‰.
2. Where quartz results from a dissolution–precipitation process at low water-to-solid ratios ($w/M = 0.01$, $\delta^{0}_{w} = 1$‰), $\delta^{18}O_{quartz}$ is relatively constant and approximates $\delta^{0}_{w} + \Delta^{0}$ (15‰).
3. Going from equilibrium to low w/M and at constant $\delta^{0}_{w} + \Delta^{0}$, $\delta^{18}O_{quartz}$ varies as family of curves of

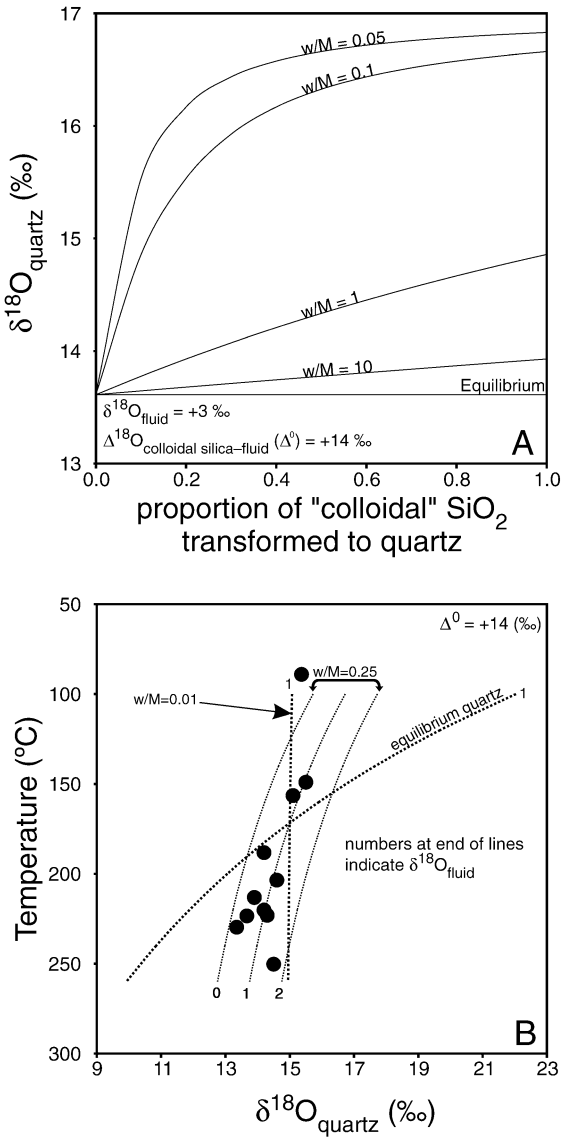

Fig. 8. Calculated variations in the bulk isotopic composition of quartz formed from the progressive dissolution–precipitation of a "colloidal" precursor. (A) Variation in $\delta^{18}O_{quartz}$ as the water to solid ratio changes from 0.05 to 10 at constant temperature (225 °C), fluid composition (+3‰) and Δ^0 (+14‰). (B) Variation in $\delta^{18}O_{quartz}$ as a function of temperature, water to solid ratio and initial fluid composition at constant Δ^0 (+14‰). Numbers on the curves refer to initial composition of the fluid (‰). Filled circles are quartz compositions and their corresponding boiling curve temperatures given in Table 1 (see text for discussion).

increasing radius of arc that pivot in an anticlockwise fashion about the intersection between the quartz equilibrium curve and $\delta^{18}O_{quartz} = \delta^0_w + \Delta^0$.

4. Changes in $\delta^0_w + \Delta^0$ at constant w/M simply shift the curve in the direction of changing $\delta^0_w + \Delta^0$ without changing the shape of the curve.

In terms of actual $\delta^{18}O_{quartz}$ compositions, we can compare the predictive curves with the measured values through the boiling curve data (Table 1). These provide a reasonable estimate of temperature–depth variation within the Profitis Ilias hydrothermal system and locate the quartz samples in temperature–$\delta^{18}O$ space. The data show an sympathetic relationship between $\delta^{18}O_{quartz}$ and temperature that is modelled by solution–precipitation processes with a water-to-solid ratio of 0.25 and, with the exception of the lowest and highest temperature samples, an initial fluid varying in composition by about 1‰ (Fig. 8B). Moreover, the data do not conform to an equilibrium model of quartz precipitation. Though kinetic processes can explain variation in $\delta^{18}O_{quartz}$ with respect to estimated paleotemperatures, relating $\delta^{18}O_{quartz}$ to $\delta^{18}O_{fluid}$ through solution–precipitation is more challenging, as this requires knowledge of $\Delta^{18}O_{silica-water}$ for the quartz precursor. In our case, a value of +14‰, taken from Kita and Taguchi (1986), predicts a fluid composition in the region of 0–1‰ (Fig. 8B). This is in approximate agreement with the sample that best reflects the reservoir composition of the hydrothermal fluid (PD9380, Table 1) and the estimated composition of the modern geothermal reservoir, but samples from higher levels record lighter values (−7.8‰) that are not predicted by solution–precipitation processes. However, these can be explained by heterogeneous trapping of liquid ($\delta^{18}O \sim 0$–1‰) and varying proportions of isotopically light vapor during boiling events (Fig. 5).

In addition, when we consider Vityk et al. (1993), kinetically controlled isotopic exchange is a much better process than posttrapping diffusion for explaining variations in $\Delta^{18}O_{corrected\text{-}FI}$. Here, variation in $\Delta^{18}O_{corrected\text{-}FI}$ is systematically related to different quartz types (Table 3). For samples where isotope and fluid inclusion temperatures agree, quartz precipitated in equilibrium with the hydrothermal fluid, or if it formed from a precursor silica phase, then fluid-to-solid ratios were high (i.e. the conditions of open

flow). For samples where isotope and fluid inclusions record different temperatures ($\Delta^{18}O_{calculated\text{-}FI}$: 2.2–8.5‰), $\Delta^{18}O_{calculated\text{-}FI}$ can be explained by quartz forming through solution–precipitation processes at low fluid-to-solid ratios (Fig. 8A). This corresponds to conditions where fluid flow was restricted and/or it underwent extensive boiling. This feature has been observed at lower temperatures by Kita and Taguchi (1986). When we consider the alternative of posttrapping diffusional exchange as a mechanism for the $\delta^{18}O$ quartz–inclusion water shift in Vityk et al. (1993), it is difficult to explain the variation. First, it would be expected to affect all samples equally. That is, for a given size of fluid inclusion, quartz age and mineralisation temperature, $\Delta^{18}O_{corrected\text{-}FI}$ should be constant in all samples. This is not the case. Some show no shift whilst others show $\Delta^{18}O_{corrected\text{-}FI}$ to be +8‰ (Table 3). In terms of a diffusion mechanism, this can only be explained by significantly different quartz ages or that fluid inclusions are significantly larger in one type of quartz. Vityk et al. (1993) do not indicate that either of these are applicable to the Beregovo quartzes.

5.5. What does fluid inclusion $\delta^{18}O$ represent?

The modelling of Dodson closure temperatures for quartz show, theoretically, that for inclusions larger than about 5 μm and at temperatures less than 250 °C, quartz does not significantly exchange $\delta^{18}O$ with fluid inclusion water. A number of independent lines of evidence support this:

1. The epithermal mineralisation at Profitis Ilias shows a consistency between $\delta^{18}O_{FI}$, δD_{FI} and fluid inclusion and geochemical data that is not seen in the $\delta^{18}O_{calculated}$ data (see Fig. 5).
2. On Milos, there is close isotopic and chemical similarity between the composition of the fluid inclusion waters and that of the modern geothermal system (see Fig. 5), and there are sound geological reasons that a continuum exists between the ancient and modern systems (Kilias et al., 2001).
3. The data of Vityk et al. (1993) record quartz–fluid inclusion isotope temperatures that agree with fluid inclusion data and cannot be explained by diffusion alone. Also, quartz and coexisting sulphides have similar δD_{FI} and $\delta^{18}O_{FI}$ (see Table 3).
4. The modelling of solution–precipitation processes show that kinetic factors are a valid alternative to posttrapping reequilibration for explaining differences between $\delta^{18}O_{calculated}$ and $\delta^{18}O_{FI}$.

Thus, the above lend support to the assertion that, in epithermal systems, $\delta^{18}O$ determined on fluid inclusion waters may be a better guide to the original isotopic composition of the hydrothermal fluid than temperature-corrected quartz data (Fig. 5). This is because $\delta^{18}O_{quartz}$ in solution–precipitation processes can be significantly different from $\delta^{18}O_{quartz}$ at equilibrium for a given temperature and $\delta^{18}O_{fluid}$. However, in higher temperature (>300 °C) hydrothermal systems, such as porphyry–Cu, Sn–W and orogenic–Au deposits, Dodson closure temperatures show that quartz and fluid inclusion water undergo posttrapping exchange. Thus, in these cases, the indirect method will always provide the best estimate of fluid $\delta^{18}O$.

Also, at Profitis Ilias, $\delta^{18}O_{FI}$ contains a record of fluid processes not seen in $\delta^{18}O_{calculated}$ (Fig. 5 and Section 5.1). First, this is probably because temperature estimates within paleohydrothermal systems are not precise enough to allow accurate reconstruction of variations in $\delta^{18}O$ of the hydrothermal fluid. For example, in a boiling epithermal system fluid, temperatures can vary by up to 50–70 °C over a vertical interval of only 100–200 m (Table 1). This can represent differences of nearly 10‰ in fluid $\delta^{18}O$ (i.e. the difference in boiling-curve-estimated $\delta^{18}O$ between 457 and 657 m elevations, Table 1). Second, formation of quartz via an amorphous precursor (e.g. Dong et al., 1995) is a non-equilibrium process and can result in estimates of $\delta^{18}O_{fluid}$ that are too heavy.

5.6. Implications for $\delta^{18}O$ analysis of quartz

At Profitis Ilias, combined δD–$\delta^{18}O_{quartz}$ and δD–$\delta^{18}O_{FI}$ and comparison with the modern geothermal system coupled with kinetic modelling of the data (Figs. 5 and 8) show that the differences in $\delta^{18}O_{quartz}$ and $\delta^{18}O_{FI}$ can be related though a combination of extensive boiling and quartz formation via an amorphous precursor. Whereas, calculation of equilibrium fluid compositions appears to overestimate the fluid composition by +8‰ to +10‰. If the kinetic model is valid, this places limitations on the use of

$\delta^{18}O_{quartz}$ in low-temperature epithermal systems to estimate $\delta^{18}O_{fluid}$ where solution–precipitation processes operate. Failure to recognise this limitation can result in significant errors in the estimation of $\delta^{18}O_{fluid}$. Observations that indicate $\delta^{18}O_{quartz}$ is kinetically controlled and mitigate against using it to calculate fluid compositions are:

1. Textural information indicating formation from an amorphous precursor (e.g. Dong et al., 1995). This can be documented through careful petrography and cathodoluminescence studies.
2. Fluid inclusion data that indicate mineralisation is associated with extensive boiling and vaporisation (e.g. Simmons and Browne, 1997; Scott and Watanabe, 1998; Kilias et al., 2001).
3. Where mineralisation temperatures are less than 250 °C and data are available. Systematic differences between $\delta^{18}O_{quartz}$ and $\delta^{18}O_{FI}$ can also indicate a kinetic control.

6. Summary and conclusions

In summary, δD and δ^{18}O in extracted fluid inclusion waters from the Profitis Ilias epithermal mineralisation were found to show a linear correlation that closely parallels the stable isotope systematics in the active Milos geothermal system, with δD varying from −23.8‰ to −68.0‰ and δ^{18}O from −0.3 to −7.8.‰. δ^{18}O analysis of the quartz, using the same samples, shows a restricted variation of 13.4–15.9‰ and correction of this data, employing a variety fluid inclusion temperature estimates, does not match δ^{18}O in the corresponding fluid inclusion waters. $\Delta^{18}O_{corrected\text{-}FI}$ ranges from +8‰ to +12‰ and calculated Dodson closure temperatures for quartz, at scales appropriate to fluid inclusions and at cooling rates compatible with the lifetime of a geothermal systems, indicate that at temperatures below 250 °C, these differences cannot be accounted for by posttrapping diffusional exchange of ^{18}O between inclusion water and host quartz. Thus, for the Profitis Ilias mineralisation, posttrapping reequilibration is not thought to be an appropriate process for explaining the observed $\Delta^{18}O_{corrected\text{-}FI}$. In our case, solution–precipitation processes are preferred as modelling shows that differences, in relative terms, between $\delta^{18}O_{FI}$ and $\delta^{18}O_{quartz}$ can be explained by kinetic processes. However, insufficient data and knowledge concerning the δ^{18}O composition of possible silica precursors at temperatures above 150 °C and fluid-to-solid ratios preclude a generalised reconstruction of fluid compositions using this method.

The results of diffusion and kinetic modelling coupled with independent lines of evidence, such as the consistency of δD_{FI} and $\delta^{18}O_{FI}$ with other geochemical data and their similarity to the isotope systematics of the modern systems, lead us to believe that fluid inclusion δ^{18}O has the potential to be a better estimator of oxygen isotope systematics in low-temperature hydrothermal systems than $\delta^{18}O_{quartz}$ and fluid inclusion temperatures. However, as there are only two published fluid inclusion δ^{18}O studies in the epithermal environment, further data from other systems are required to extend the applicability our findings. In the first instance, these should concentrate on boiling systems as these provide the best temperature constraints. In addition, good petrographic and geologic control is a prerequisite for reliable interpretations. In our case, this was achieved through detailed petrography and fluid inclusion microthermometry within a well-constrained spatial and geological framework (Kilias et al., 2001) that enabled comparisons between a mineralised system and its modern analogue. At a smaller scale, or in the absence of a modern analogue for comparison, careful cathodoluminescence petrography coupled with localised isotopic analysis of the quartz will also fulfil the requirement. Finally, recent analytical developments for the rapid determination of δD and δ^{18}O in small (0.1 μl) amounts of water (Sharp et al., 2001) indicate it should be possible to routinely analyse inclusion waters without the need for the lengthy sample preparation and analytical procedures. Factors that have so far hindered systematic investigations into the applicability of oxygen isotope determination of fluid inclusion water.

Acknowledgements

This work was funded by the British Council, The Greek General Secretariat of Research and a Marie Curie Experienced Researcher Fellowship to JN (HPMF-CT-2000-00762). Special thanks go to J.A.

Crossing and Y. Simos, geologists at Midas S.A., who allowed access to drill-core and proprietary company data. Drs. T.H.E. Heaton and B. Spiro are thanked for providing impetus and encouragement during the research. J.N., M.J.L. and T.J.S. publish with the permission of the Director, British Geological Survey (NERC). **[CA]**

References

Bodnar, R.J., Reynolds, T.J., Kuehn, C.A., 1985. Fluid inclusion systematics in epithermal systems. In: Berger, B.R., Bethke, P.M. (Eds.), Geology and Geochemistry of Epithermal Systems. Rev. Econ. Geol., vol. 2, pp. 73–97.

Briqueu, L., Javoy, M., Lancelot, J.R., Tatsumoto, M., 1986. Isotope geochemistry of recent magmatism in the Aegean arc: Sr, Nd, Hf, and O isotopic ratios in the lavas of Milos and Santorini—geodynamic implications. Earth Planet. Sci. Lett. 80, 41–54.

Christanis, K., St. Seymor, K.S., 1995. A study of scale deposition an analog of mesothermal to epithermal one formation in the volcano of Milos, Agean-arc, Greece. Geothermics 24, 541–552.

Clayton, R.N., Mayeda, T.K., 1963. The use of bromine pentafluoride in the extraction of oxygen from oxide and silicates for isotopic analysis. Geochim. Cosmochim. Acta 27, 43–52.

Craig, H., 1957. Isotopic standards for carbon and oxygen and correction factors for mass spectromatic analysis of carbon dioxide. Geochim. Cosmochim. Acta 12, 133–149.

Deines, P., 1970. Mass spectrometer correction factors for the detection of small isotopic variation of carbon and oxygen. Int. J. Mass Spectrom. Ion Phys. 4, 283–295.

Dodson, M.H., 1973. Closure temperature in cooling geochronological and petrologic systems. Contrib. Mineral. Petrol. 40, 259–274.

Dodson, M.H., 1979. Theory of cooling ages. In: Jaeger, E., Hunziker, J.C. (Eds.), Lectures in Isotope Geology. Springer-Verlag, Heidelberg, pp. 194–202.

Dong, G., Morrison, G., Jaireth, S., 1995. Quartz textures in epithermal veins, Queensland-classification, origin and implication. Econ. Geol. 90, 1841–1856.

Dubinina, E.O., Lakshtanov, L.Z., 1997. A kinetic model of isotopic exchange in dissolution–precipitation processes. Geochim. Cosmochim. Acta 61, 2265–2271.

Farver, J.R., Yund, R.A., 1991. Oxygen diffusion in quartz: dependence on temperature and water fugacity. Chem. Geol. 90, 55–70.

Fytikas, M., 1989. Updating of the geological and geothermal research on Milos island. Geothermics 18, 485–496.

Haas Jr., J.L., 1977a. Physical properties of the coexisting phases and thermochemical properties of the H_2O component in boiling NaCl solutions. U.S. Geol. Surv. Prof. Pap., B 1421-A, A1–A73.

Haas Jr., J.L., 1977b. Thermodynamic properties of the coexisting phases and thermochemical properties of the NaCl component in boiling NaCl solutions. U.S. Geol. Surv. Prof. Pap., B 1421-B, B1–B71.

Hayashi, K.-I., Maruyama, T., Satoh, H., 2001. Precipitation of gold in a low-sulfidation epithermal gold deposit: insights from a submillimeter-scale oxygen isotope analysis of vein quartz. Econ. Geol. 96, 211–216.

Hedenquist, J.W., Reyes, A.G., Simmons, S.F., Taguchi, S., 1992. The thermal and geochemical structure of geothermal and epithermal systems: a framework for interpreting fluid inclusion data. Eur. J. Mineral. 4, 989–1015.

Horita, J., Cole, D.R., Wesolowski, D.J., 1995. The activity–composition relationship of oxygen and hydrogen isotopes in aqueous salt solutions: III. Vapor–liquid water equilibration of NaCl solutions to 350 °C. Geochim. Cosmochim. Acta 59, 1139–1151.

Kazahaya, K., Matsuo, S., 1984. A new ball-milling method for extraction of fluid inclusions from minerals. Geochem. J. 19, 45–54.

Kilias, S., Naden, J., Cheliotis, I., Shepherd, T.J., Constandinidou, H., Crossing, J., Simos, I., 2001. Epithermal gold mineralisation in the active Aegean Volcanic arc: the Profitis Ilias deposit, Milos island, Greece. Miner. Depos. 36, 32–44.

Kishima, N., Sakai, H., 1980. Oxygen-18 and deuterium determinations on a single water sample of a few milligrams. Anal. Chem. 52, 356–358.

Kita, I., Taguchi, S., 1986. Oxygen isotopic behavior of precipitating silica from geothermal water. Geochem. J. 20, 153–157.

Lecuyer, C., O'Neil, J.R., 1994. Stable isotope compositions of fluid inclusions in biogenic carbonates. Geochim. Cosmochim. Acta 58, 353–363.

Liakopoulos, A., 1987. Hydrothermalisme et mineralisations metalliferes de l'ile de Milos (Cyclades–Grece). Mem. Sci. Terre. Universite Paris, VI, No. 36–87.

Liakopoulos, A., Katerinopoulos, A., Markopoulos, T., Boulegue, J., 1991. A mineralogical, petrographic and geochemical study of samples from wells in the geothermal field of Milos Island (Greece). Geothermics 20, 237–256.

Lüders, L., Pracejus, B., Halbach, P., 2001. Fluid inclusion and sulfur isotope studies in probable modern analogue Kuroko-type ores from the JADE hydrothermal field (Central Okinawa Trough, Japan). Chem. Geol. 173, 45–58.

Matsuhisa, Y., Goldsmith, J.R., Clayton, R.N., 1978. Mechanisms of hydrothermal crystallization of quartz at 250 °C and 15 kbar. Geochim. Cosmochim. Acta 42, 173–182.

Ohba, T., Matsuo, S., 1988. Precise determination of hydrogen and oxygen isotope ratios of water in fluid inclusions of quartz and halite. Geochem. J. 22, 55–68.

Ohba, T., Kazahaya, K., Matsuo, S., 1995. Diffusional ^{18}O loss from inclusion water in a natural hydrothermal quartz from the Kaneuchi tungsten deposit, Japan. Geochim. Cosmochim. Acta 59, 3039–3047.

O'Neil, J.R., Adami, L.H., Epstein, S., 1975. Revised value for the ^{18}O fractionation between CO_2 and water at 25 °C. J. Res. U.S. Geol. Surv. 3, 623–624.

O'Reilly, C., Jenkin, G.R.T., Feely, M., Alderton, D.H.M., Fallick, A.E., 1997. A fluid inclusion and stable isotope study of fluid

evolution in the Galway Granite, Connemara, Ireland. Contrib. Mineral. Petrol. 129, 120–142.

Papazachos, C.B., Kiratzi, A.A., 1996. A detailed study of the active crustal deformation in the Aegean and surrounding area. Tectonophysics 253, 129–153.

Pflumio, C., Boulegue, J., Liakopoulos, A., Briqueu, L., 1991. Oxygen, hydrogen, strontium isotopes and metals in the present-date and past geothermal systems of Milos island (Aegean arc). In: Pagel, M., Leroy, J.L. (Eds.), Source, Transport and Deposition of Metals. Balkema, Rotterdam, pp. 107–112.

Pichavant, M., Ramboz, C., Weisbrod, A., 1982. Fluid immiscibility in natural processes; use and misuse of fluid inclusion data: I. Phase equilibria analysis; a theoretical and geometrical approach. Chem. Geol. 37, 1–27.

Ramboz, C., Pichavant, M., Weisbrod, A., 1982. Fluid immiscibility in natural processes; use and misuse of fluid inclusion data: II. Interpretation of fluid inclusion data in terms of immiscibility. Chem. Geol. 37, 29–48.

Rye, R.O., O'Neil, J.R., 1968. The O^{18} content of water in primary fluid inclusions from Providencia, north-central Mexico. Econ. Geol. 63, 232–238.

Scott, A.M., Watanabe, Y., 1998. "Extreme boiling" model for variable salinity of the Hokko low-sulfidation epithermal Au prospect, southwestern Hokkaido, Japan. Miner. Depos. 33, 568–578.

Sharp, Z.D., Atudorei, V., Durakiewicz, T., 2001. A rapid method for determination of hydrogen and oxygen isotope ratios from water and hydrous minerals. Chem. Geol. 178, 197–210.

Sheppard, S.M.F., 1986. Characterization and isotopic variations in natural waters. In: Valley, J.W., Taylor, Jr., H.P., O'Neil, J.R. (Eds.), Stable Isotopes in High Temperature Geological Processes. Reviews in Mineralogy, vol. 16. Mineralogical Society of America, Washington, DC, pp. 165–183.

Simmons, S.F., Browne, P.R.L., 1997. Saline fluid inclusions in sphalerite from the Broadlands-Ohaaki geothermal system: a coincidental trapping of fluids being boiled toward dryness. Econ. Geol. 92, 485–489.

Truesdell, A.H., 1984. Stable isotopes in hydrothermal systems. In: Henley, R.W., Truesdell, A.H., Barton, P.B. (Eds.), Fluid–Mineral Equilibria in Hydrothermal Systems. Rev. Econ. Geol., vol. 1, pp. 129–142.

Tsokas, G.N., 1996. Interpretation of the Bouguer anomaly of Milos island (Greece). J. Volcanol. Geotherm. Res. 72, 163–181.

Valley, J.W., 2001. Stable isotope thermometry at high temperatures. In: Valley, J.W., Cole, D.R. (Eds.), Stable Isotope Geochemistry. Rev. Mineral. Geochem., vol. 43, pp. 365–413.

Vityk, M.O., Krouse, H.R., Demihov, Y.N., 1993. Preservation of $\delta^{18}O$ values of fluid inclusion water over geological time in an epithermal environment: Beregovo deposit, Transcarpathia, Ukraine. Earth Planet. Sci. Lett. 119, 561–568.

Wilkinson, J.J., Jenkin, G.R.T., Fallick, A.E., Foster, R.P., 1995. Oxygen and hydrogen isotopic evolution of Variscan crustal fluids, south Cornwall, UK. Chem. Geol. 123, 239–254.

Zhang, L., Liu, J.X., Zhou, H., Chen, Z.S., 1989. Oxygen isotope fractionation in the quartz–water–salt system. Econ. Geol. 84, 1643–1650.